Received: 11 October 2016 | Revised: 10 April 2017 | Accepted: 28 June 2017

DOI: 10.1002/stc.2071

RESEARCH ARTICLE

WILEY

Wavelet energy ratio index for health monitoring of hysteretic dampers

Elisabet Suarez[1] | Amadeo Benavent-Climent[2] | Ruben Molina-Conde[1] | Antolino Gallego[1]

[1] Department of Applied Physics, University of Granada, Campus Fuentenueva, 18071 Granada, Spain

[2] Department of Mechanical Engineering, Technical University of Madrid, C/ José Gutierrez Abascal, 2, 28006 Madrid, Spain

Correspondence
Elisabet Suarez, Department of Applied Physics, University of Granada, Campus Fuentenueva, 18071 Granada Spain.
Email: elisabetsv@ugr.es

Summary

This paper presents new contributions to evaluate the damage suffered on a particular type of hysteretic damper called web plastifying damper (WPD) for the passive control of structures subjected to earthquakes. WPDs consist of several I-section steel segments arranged to form a brace-type structural element. Energy input by the earthquake is dissipated by the WPD through plastic deformations of the web of the I-sections. These devices, properly installed in reinforced concrete test models, were tested under successive seismic simulations of increasing magnitude with a shaking table. To assess the damage of the web of the I-section after each seismic simulation, a new damage index called *wavelet energy ratio* (WER) was developed; it uses the signals collected by piezoelectric sensors in simple vibration tests. The index is based on wavelet package decomposition and energy calculation of properly chosen wavelet coefficients. It was correlated with a mechanical energy-based damage index—ID—proposed in past research, which has proven to accurately characterize the level of damage yet requires costly instrumentation to acquire the load–displacement curve needed for its computation. The experiments reported in this paper demonstrate a good correlation between WER and ID indices in a realistic seismic loading scenario. On the basis of this correlation, it is possible to estimate ID indirectly from the WER, which involves much simpler and less expensive instrumentation, easily applicable for in situ continuous monitoring of the dampers.

KEYWORDS

hysteretic dampers, seismic loads, structural health monitoring, vibration tests, wavelet

1 | INTRODUCTION

Passive control of structures subjected to seismic actions through the use of energy dissipating devices (EDD) is becoming a popular solution in earthquake-prone areas. A typical building structure with passive control systems consists of a main frame —designed for sustaining principally the gravity loads—that works in conjunction with special elements called EDDs or simply dampers, whose main role is to dissipate most of the energy input from the earthquake. Among the different types of EDDs available (viscous dampers, friction dampers, viscoelastic dampers, etc.), the so-called *hysteretic dampers* are probably the most widely used due to their advantages in terms of robustness, reliability, and cost. The source of energy dissipation

through hysteretic dampers is the plastic deformation of metals (commonly steel). However, inelastic strains in the material imply damage. Evaluating the level of damage to the hysteretic dampers after a seismic event is a matter of great concern, because the decision of whether or not to replace the EDDs has important economic and safety-related consequences. Hysteretic dampers do not necessarily need to be replaced after minor/moderate damage, or even after a large earthquake, because they possess a high energy dissipation capacity. Still, a reliable evaluation of the level of damage is essential for determining the remaining energy dissipation capacity (life) of the damper.

Damage evaluation of hysteretic dampers caused by the plastic deformation of steel cannot be based on simple visual inspection because it is a cumulative process, not visible until the element is on the brim of failure. Past research has shown that the level of damage and the proximity to failure of hysteretic dampers subjected to arbitrarily applied cyclic loading can be reliably estimated by decomposing the force-displacement curves endured by the damper into the so-called *skeleton and Bauschinger parts*.[1] This decomposition is the basis of a mechanical damage index called ID that has been extensively validated with static and dynamic tests. Yet measuring the force and the displacement of dampers during an earthquake involves installing expensive instrumentation (load cells or strain gauges and displacement transducers) that would offset one of their main advantages—low cost. Further, such instrumentation is hardly justified when the probability of occurrence of an earthquake is very low.

An alternative is to use piezoceramic sensors permanently attached to the hysteretic damper and conduct simple vibration tests.[2–5] Piezoceramic sensors are low-cost devices that can both excite and measure the response of the structural element whose health is to be assessed. Vibration-based damage detection strategies are based on the correlation between the vibration response of the structure and the presence of damage.[6] Damage due to plastic deformations induces changes in the vibration response (resonance frequencies, modes, damping coefficients, etc.) that can be evaluated through a proper processing of signals captured by piezoceramic sensors and correlated with presence (Level 1 in structural health monitoring, SHM), position (Level 2 in SHM) and intensity of damage (Level 3 in SHM). Although many papers in the literature deal with time vibration series analysis for damage detection in structures and materials,[6,7] it is worth noting that none of these techniques has been applied to evaluate the damage on hysteretic dampers, comparing and correlating it with that of mechanical indexes of damage.

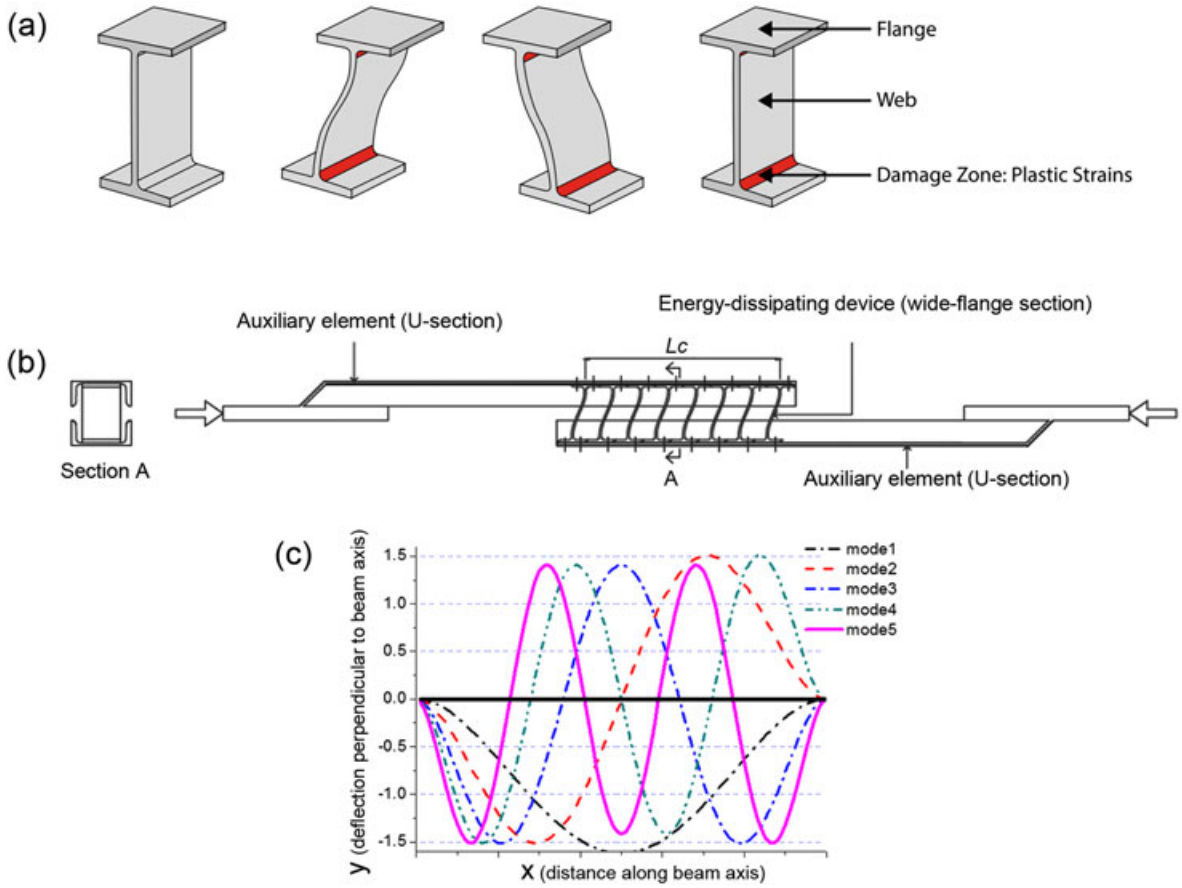

FIGURE 1 (a) I-shape steel segment and deformation pattern; (b) web plastifying damper; (c) modal shapes of beam with fixed ends

This paper proposes a new index named WER to evaluate the damage suffered on a particular type of hysteretic damper known as web plastifying damper (WPD), developed by the authors.[8] The WER index uses the signals measured by piezoceramic sensors in simple vibration tests, and it is based on wavelet package decomposition and energy calculation of properly chosen wavelet coefficients obtained from these signals. Wavelet transform of vibration signals has been widely used for structural damage detection.[9–24] Basically, by means of the wavelet decomposition of the time-domain signal on the time-frequency domain, it is possible to observe dominant modes of variability of the signal (frequencies) and how these modes vary along the time. Especially, researchers have been trying to develop approaches that provide enough feasibility of small damages detection. Previous results have proved that the energy of the decomposed wavelet vibrational signals using the wavelet packet has higher sensitivity to small damage.[22–24] The wavelet packet decomposition is an effective way of searching over wide frequency band for weak change signals induced by the damage. It is well known that traditional Fourier-based methods have been used for this purpose over several decades. In particular, for damage evaluation of WPD dampers, as reported in this paper, the authors have previously proposed and validated the use of the area damage index, based on the evaluation of changes in the frequency response function (FRF) calculated by means of the Fourier analysis.[2–5] This paper demonstrates that the change induced by the damage is more clearly observable on the damage vector used to calculate the new index WER than on the FRF magnitude. In other words, the resolution in frequency required to evaluated changes in the signal produced by damage is much higher than required for the wavelet-based index.

The WPD consists of several short segments of I-shape steel sections, shown in Figure 1(a), mounted on auxiliary steel elements to form a brace-type structural member, Figure 1(b). The I-shape steel segments are arranged so that when the brace-type member is loaded in the direction of its axis, the web of the I-shape steel segments is subjected to out-of-plane bending deformations. The web of an I-shape steel section and its boundary conditions within the WPD device can be modeled as a beam with both ends fixed. Figure 1(c) shows the first five modal shapes of a continuous beam with fixed ends. The reason behind energy dissipation in the WPDs is the plastification of the web of the steel I-section. The relatively low stiffness and size of the I-shape steel sections makes it possible to excite them with small-size piezoceramic sensors.

The WER index has been validated experimentally with dynamic shaking table tests conducted on several WPDs. A very good correlation was found between the WER index and the mechanical damage index ID proposed in past research. Moreover, the WER index can reliably evaluate the level of damage on WPDs without the need of knowing the load–displacement relationship endured by the damper and thus without resorting to the cumbersome and expensive instrumentation required to obtain the ID.

2 | SPECIMEN DESCRIPTION

First, two reinforced concrete prototype structures having three stories and 3 × 3 bays were designed to sustain the gravity loads established under current codes in Spain. One prototype consisted of a frame structure and the other a flat-slab structure. Each prototype was equipped with WPDs designed to sustain the seismic loads prescribed by the Spanish Seismic code. From each prototype, a test model that represented a portion of the prototype structure was defined and constructed by applying a scaling factor of 2/5 to the geometry. The test model that represented the frame structure is called specimen FD, and it is shown in Figure 2(a). The test model that represents the flat-slab structure is named specimen SD and it is shown in Figure 2(b). Each test model has two levels; the lowest level will be referred to as ground floor, and the highest one as first floor herein. A detailed description of the test structures can be found in the literature.[25,26] Specimen FD was equipped with four WPDs, two on the first level and two on the second level. Specimen SD was equipped with two WPDs, one on each floor.

3 | DESCRIPTION OF THE EXPERIMENTS

3.1 | Shaking table tests

The two test models described in the previous section were mounted on the uniaxial 3 × 3 m^2 shaking table of the University of Granada, as shown in Figure 2, and subjected to successive seismic simulations of increasing amplitude. The lateral displacements induced in the test model during each simulation imposed forced axial deformations on the WPDs that damaged the I-section steel segments. In each seismic simulation, the shaking table

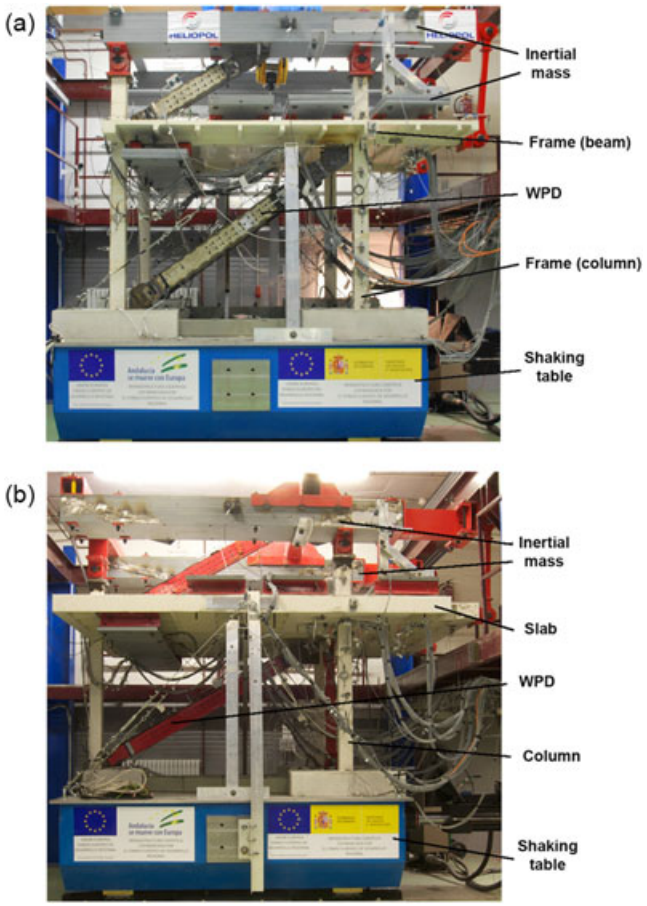

FIGURE 2 Overview of test models and setup on the shaking table. (a) FD specimen; (b) SD specimen

reproduced the ground motion acceleration recorded at Calitri during the Campano Lucano earthquake (1980), scaled in amplitude to different levels. The scaling factors applied to test model FD were 100%, 200%, 300%, and 350% times the acceleration of the original record, and the corresponding peak ground accelerations were 0.16 *g*, 0.31 *g*, 0.47 *g*, and 0.54 *g* (here *g* is the acceleration of gravity). The respective levels of damage on the WPDs at the end of each seismic simulation will hereafter be identified as d0, d1, d2, and d3. The scaling factors applied to test model SD were 100%, 200%, 300%, 400%, 500%, and 600% times the acceleration of the original record, and the corresponding levels of damage will be identified as d0, d1, d2, d3, d4, and d5 hereafter. For illustrative purposes, Figure 3 shows the histories of acceleration applied to specimen FD. The test models and the WPDs were instrumented with displacement transducers, strain gauges and accelerometers.

3.2 | Forced vibration tests

Vibration tests were carried out on several I-shape steel segments at the end of each seismic simulation, when the shaking table and the specimen stopped moving. The instant when these tests were conducted is indicated with a square symbol in Figure 3. To this end, prior to application of the seismic simulations described above, several I-section steel segments were instrumented with two piezoelectric ceramic sensors (PZTs) attached to the web. One PZT (model PI®PRYY0842) worked as the actuator and was attached at the center of the web of the I-section; the other PZT (model PI®PRYY + 0220) worked as the sensor and was attached just opposite the first. The center of the web I-section is the region undergoing a minimal level of deformation, so as to avoid damaging the PZTs. Moreover, it was corroborated that in this area, the sensor is able to detect all the resonant frequencies.[2] It is worth emphasizing that the vibration tests can be carried out at any moment in the service life of a structure.

The signals generated in these vibration tests were recorded by means of the electronic measurement system shown in Figure 4. The equipment included a computer and a system of connections. The I-section was excited with white noise

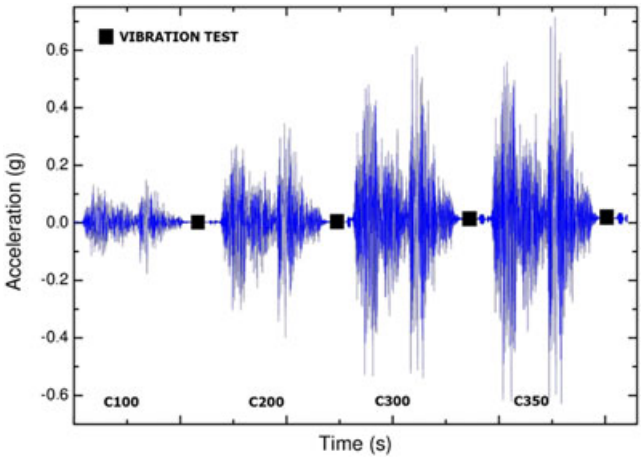

FIGURE 3 Accelerations of the seismic simulations applied to the structure FD

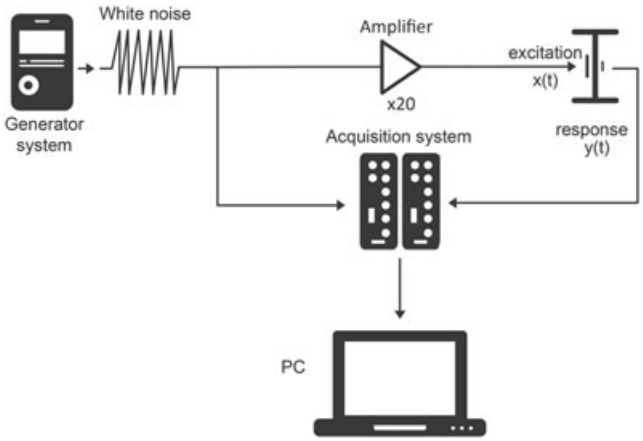

FIGURE 4 Scheme of electronic measurement system in laboratory

generated by CoCo80 equipment (*CRYSTAL Instruments*). However, the signal proved insufficient to properly excite the I-sections, making it necessary to use an *EPA104* piezoelectric amplifier that provided a gain of 20. Each vibration test was carried out four times with different white noise realizations. The duration of each test was 20 s, and the sampling rate of signals was 65536 Hz. The response signal of the I-sections was recorded by two PULSE 3560-B *Brüel & Kjær* systems.

All electronic devices were properly connected to the grounding system; connections were made so that the measurement system would achieve a good performance against the electrical and environmental noises. In this way, a robust measurement system was obtained, with controlled noise conditions and high-quality vibration signals.

4 | PROPOSED DAMAGE INDEX—FORMULATION

In this study, a method based on wavelet packet transform (WPT) is proposed for damage evaluation of WPDs. The WPT-based method consists of two steps. The first one is to decompose the vibration signals measured from I-sections into wavelet packet components. The second step is to calculate component energies and compute a WER that is proposed here as a damage index. Various levels of damage assessment are studied.

4.1 | Background of the wavelet packet transform (WPT) technique

Wavelet packet transform is one extension of the wavelet transform to decompose a signal repeatedly into successive low- and high-frequency components. It differs from wavelet multiresolution analysis (WMRA) in that not only is the

approximation at a given level decomposed further but also are the details. This results in a more flexible and wider base for the analysis of monitored signals.[27,28]

A wavelet packet is a family of scaling functions and wavelet functions constructed by following a binary tree of dilations/translations. A wavelet packet, $\psi^i_{j,k}(t)$, is a function of three indices, where i, j, and k are integers representing the modulation, the scale, and the translation parameters, respectively. It can be written as[27–32]

$$\psi^i_{j,k}(t) = 2^{j/2}\psi^i\left(2^j t - k\right), \qquad i = 1, 2, 3\ldots, \tag{1}$$

where $\psi^i(t)$ is the mother wavelet function. There are quite a few mother wavelets reported in the literature, developed to satisfy some important properties such as invertibility and orthogonality.[31,32] Daubechies[30] developed a family of mother wavelets on the basis of the solution of a dilation equation. In the present work, among several alternatives, Daubechies functions of the order 5 (db5) were selected as mother wavelets on the basis of trial and error tests.

The analytical procedure starts by computing the wavelet packet decomposition of the monitored vibration signal at level N using a given wavelet. This means that there are 2^N components at the Nth level, providing flexibility for choosing the way to encode the original signal, so that the reconstruction error is minimal. A schematic representation of the WPT of a time-domain signal $f(t)$ up to the third level of decomposition is presented in Figure 5; it can be obtained, for instance, by summing the signal components $f^1_1(t), f^5_3(t), f^6_3(t)$, and $f^4_2(t)$. The approximations correspond to the low scale (low-frequency components) of the signal, whereas the details correspond to the high scale (high-frequency components) of the signal.

It is worth mentioning that a downsampling process is performed at every decomposition stage. If the decomposition operation is performed on the entire range of the signal, the number of samples considered in the analysis will be doubled. That is, if the original signal consists of 100 samples, the approximation and the detail signals will each have 100 samples (200 samples total). In order to overcome this problem, which affects computation time and data storage, the downsampling process is carried out ignoring the second sample of each sampling pair.

After j levels of decomposition, the original signal $f(t)$ can be expressed as[28]

$$f(t) = \sum_{i=1}^{2^j} f^i_j(t), \tag{2}$$

where $f^i_j(t)$ is the subsignal with the orthogonal frequency band, i is the number of the node, and j indicates the level of decomposition of the tree structure. The wavelet packet component signal $f^i_j(t)$ can be expressed by a linear combination of wavelet packet functions $\psi^i_{j,k}(t)$ as follows[28]

$$f^i_j(t) = \sum_{k=-\infty}^{\infty} c^i_{j,k}\psi^i_{j,k}(t), \tag{3}$$

where the wavelet packet coefficients $c^i_{j,k}$ can be obtained from[28]

$$c^i_{j,k} = \int_{-\infty}^{\infty} f(t)\psi^i_{j,k}(t)dt. \tag{4}$$

Each component in the WPT tree can be viewed as the output of a filter tuned to a particular basis function, so that the whole tree can be regarded as a filter bank. At the top of the WPT tree (lower level), the WPT yields good resolution in the time domain but poor resolution in the frequency domain. At the bottom of the WPT tree (higher level), the WPT results in good resolution in the frequency domain but poor resolution in the time domain.

The frequency ordering of wavelet packet coefficients is not in a succession but rather in binary Gray code order. This is because the output of any two-channel analysis is the result of low/high pass filtering followed by downsampling. The

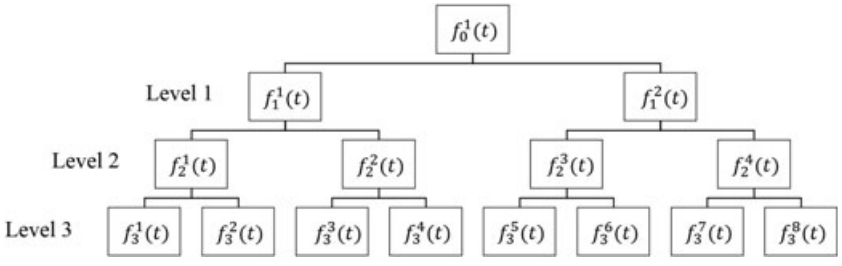

FIGURE 5 Schematic representation of three wavelet packet transform levels of a signal

downsampling generates two new filter results with half the number of elements. In addition, it results in a mirroring of the high-pass components. This switches the order of low- and high-pass components in a subsequent decomposition. When the wavelet packet algorithm is recursively applied, the frequency ordering of the resultant carriers follows the Gray code sequence.[33] This factor must be considered during the identification of used/unused bands.

4.2 | Proposal of wavelet energy ratio (WER)

In this subsection, a procedure and a formulation are proposed to obtain a new damage index called the WER to evaluate the level of damage of the I-section steel segments that form the WPDs when subjected to arbitrarily applied seismic-type dynamic loadings. The WER index is based on the energy evaluation of the WPT, and the procedure involves two phases that must be conducted prior to and after damaging the damper. The first (referred to as Phase 0 herein) consists of characterizing the undamaged I-section steel segments through vibration tests (characterization phase). The next one (referred to as Phase I) consists of conducting vibration tests at any moment during the service life of the I-sections (inspection phase) to assess their "health".

In order to extract the structural damage information from the recorded signals obtained by vibration tests and to calculate the WER index of damage, the following steps are taken:

1. First, normalization and scaling must be applied to counteract different excitation levels and environmental conditions and to compensate the offset and amplitude variability among signals. More precisely, this normalization is carried out as follows:

$$f(t) = \frac{f(t)_r - \overline{f}(t)_r}{\sigma\left(f(t)_r\right)}, \tag{5}$$

where $f(t)$ is the normalized signal, $f(t)_r$ is the recorded signal, and $\overline{f}(t)_r$ and $\sigma(f(t)_r)$ are the mean value and the standard deviation of the $f(t)_r$, respectively.

2. The normalized signal $f(t)$ is decomposed into multiple subsignals in various frequency bands using the WPT. Let $f_0^1(t)$ denote the normalized response signal, shown in Equation 2. Through trial and error tests, it was found that the optimum level of decomposition is 7; thus, 2^7 (128 nodes) is the number of subsignals to be obtained in the proposed procedure. This step must be carried out in both Phase 0 and Phase I.
3. The energy of each subsignal is calculated according to the following equation

$$E_j^i = \int \left| f_j^i(t) \right|^2 dt. \tag{6}$$

This provides the energy E_j^{i0} for the undamaged I-section and energy E_j^i for the inspected I-section, where i is the number of the node and j is the level of decomposition.

4. The energy of each subsignal obtained during the vibration test in Phase I (E_j^i) is compared with the energy of the subsignal at the same position (j,i) obtained in Phase 0 (E_j^{i0}). The magnitude of variation of the ith order subsignal energy is characterized by the parameter Λ_i defined by Equation 7, which is a measurement of the enhancement or attenuation of the ith order subsignal energy.

$$\Lambda_i = 1 - \frac{E_j^{i0}}{E_j^i} \quad i = 1, 2, \ldots, 2^j. \tag{7}$$

5. A nondimensional index vector is composed as follows:

$$V_d = [\Lambda_1, \Lambda_2, \ldots, \Lambda_{128}]. \tag{8}$$

6. Finally, the WER index is defined as the value of the largest component of the index vector, considering a frequency band around 25 kHz, corresponding with the fifth frequency of resonance of the I-sections,[2–4] that is, the maximum resonance frequency of the I-sections recorded with the measurement equipment. As can be seen in Figure 1(c), among the first five vibration modes, the fifth mode is the one that presents the maximum displacements and strains closest to beam ends. When the WPD is subjected to forced deformations in the direction of its axis, the maximum strains and the subsequent plastic deformations occur at both ends of the web of the I-shape section as shown in Figure 1(a). The fifth mode is therefore the most "sensible" to stiffness variations near the ends of the web of the I-section due to the development of plastic strains. This fact justifies mechanically why the damage is visible in the WPT frequency band around the fifth natural frequency of the I-sections. The signal was divided into 128 nodes, meaning each node includes a frequency band of 256 Hz. The index vector V_{d} corresponding with this frequency band is called V_{d}^5 and includes the band [24576, 26112] Hz. Thus,

$$V_{\mathrm{d}}^5 = V_{\mathrm{d}}\,[24576,\ \ 26112]\ \mathrm{Hz} = [\Lambda_{97}, \Lambda_{98}, \Lambda_{99}, \Lambda_{100}, \Lambda_{101}, \Lambda_{102}]. \tag{9}$$

$$\mathrm{WER} = \max\left[V_{\mathrm{d}}^5\right] = \max[\Lambda_{97}, \Lambda_{98}, \Lambda_{99}, \Lambda_{100}, \Lambda_{101}, \Lambda_{102}]. \tag{10}$$

5 | RESULTS

5.1 | Mechanical behavior of the dampers and mechanical damage index ID

The strain gauges and the displacement transducers installed in the WPDs made it possible to calculate the axial force N and the axial displacement δ endured by the WPD, at each instant t_i of the dynamic tests described in Section 3. The $N-\delta$ curve exhibited by each WPD up to a given point of the loading process, defined by its coordinate $(V_i-\delta_i)$, can be decomposed into the so-called skeleton part and the Bauschinger part.[1] For each domain of loading, the skeleton part is formed by connecting sequentially the segments of the $N-\delta$ curve in which N exceeds the maximum axial force attained by the WPD in previous cycles of loading. The remaining part of the $N-\delta$ curve is the Bauschinger part. For each domain of loading, the area enveloped by the skeleton curve up to a given point, (V_i, δ_i), will be called ${}_sW_i^+$ for the positive domain and ${}_sW_i^-$ for the negative domain. Similarly, the area enveloped by the Bauschinger curve up to a given point (V_i, δ_i) will be called ${}_BW_i^+$ for the positive domain and ${}_BW_i^-$ for the negative domain. The sums ${}_sW_i^+ + {}_BW_i^+$ in the positive domain, and ${}_sW_i^- + {}_BW_i^-$ in the negative domain, represent the total plastic strain energy dissipated by the WPD in each domain of loading. For convenience, these energies can be expressed in nondimensional form in terms of the new ratios, $\overline{\eta}_i^+$, $\overline{\eta}_i^-$, defined as follows:

$$\overline{\eta}_i^+ = \frac{{}_sW_i^+ + {}_BW_i^+}{N_y\delta_y}; \qquad \overline{\eta}_i^- = \frac{{}_sW_i^- + {}_BW_i^-}{N_y\delta_y}. \tag{11}$$

Here, N_y and δ_y are the axial force and the axial displacement at yielding. Using these ratios, the level of mechanical damage accumulated in a metallic hysteretic damper subjected to arbitrarily applied cyclic loading up to an instant t_i can be predicted with the index ID defined by[1]:

$$\mathrm{ID}_i = \max\left\{\overline{\mathrm{ID}}_i^+, \overline{\mathrm{ID}}_i^-\right\}, \tag{12}$$

where

$$\overline{\mathrm{ID}}_i^+ = \frac{\overline{\eta}_i^+}{\overline{\eta}_u^+}; \qquad \overline{\mathrm{ID}}_i^- = \frac{\overline{\eta}_i^-}{\overline{\eta}_u^-}. \tag{13}$$

In Equation 13, $\overline{\eta}_u^+$ and $\overline{\eta}_u^-$ represent the ultimate energy dissipation capacity of the EDD related to the material properties of the steel and the geometry of the WPD, and they must be determined experimentally. A detailed explanation of how they are calculated and their values for the WPD investigated in this study can be found in Benavent et al.[8] The value $\mathrm{ID}_i = 0$ indicates no damage, whereas $\mathrm{ID}_i = 1$ means complete failure.

5.2 | WER versus ID damage indices

Four dampers were installed at the FD specimen, which consisted in two frames. In each frame two dampers were used, one in each floor (ground and first floors). Dampers at the ground floor had 10 I-sections, whereas dampers at the first floor had 8 sections. For saving time and money, only six I-sections were instrumented with piezoelectric sensors. Four of them corresponded to the dampers of one frame (two at each floor), and four of them corresponded to the dampers of the other frame (one at each floor). For dampers with two I-sections instrumented, I-sections were selected to be placed around the center and at the end of dampers.

Specimen SD had only two dampers, one at the ground floor (with 20 I-sections) and other at the first floor (with 15 I-sections). Four I-sections of each damper were instrumented with piezoelectric transducers, two around the center and two around the ends of the dampers.

In this paper, for brevity reasons, only the results corresponding to two I-sections in each floor for both specimens are presented, that is, four I-sections for each specimen (FD and SD). The values of the mechanical damage index ID_i at the end of each seismic simulation are shown in Tables 1 and 2, for the dampers of the selected I-sections. In this table, the level of damage at the end of the simulation is identified as d0, d1, d2, d3, d4, or d5, as explained in Section 3.1. Note that although ID index will be the same for all the I-sections of one damper (it makes evaluation of damage of the whole damper), WER index will be different, because vibration tests are carried for each particular I-section and each I-section will have different level of damage. On the other hand, for statistical reasons, each vibration test—conducted before and after seismic simulations—was repeated four times and the average data were used. Average was carried out on computed indices V_d, not on the time signals used to compute them.

Figure 6 shows the V_d vector obtained for the different levels of damage as function of the frequency, for four I-sections of specimen FD. A substantial and clear increase of V_d is observed around 25 kHz, corresponding with the higher registered resonance frequency of the I-sections. One premise of SHM based on vibration analysis is that a change in the mechanical properties produces a change in the dynamic characteristics of the system. In general, it is very well known that as the order of the resonance frequency increases, the change in terms of dynamic characteristics will become greater. In this frequency band, it is clear that V_d increased when the seismic acceleration applied by the shaking table increased. For this reason, the frequency band [24576, 26112] Hz was selected to calculate the WER index.

For comparison with the use of the Fourier analysis, Figure 7 shows the FRF magnitude in the range [0–32] kHz and zoomed over the narrow range around the fifth resonance, for the section I1 placed on the ground floor of the specimen FD. It can be seen that the change induced by the damage is more clearly observable on the V_d damage vector than on the FRF magnitude. These differences are evaluated on Table 3, which shows in percentage the changes in amplitude of the V_d vector and the changes in amplitude of the FRF, respect to the seismic simulation C100. Differences are significantly greater for damage vector V_d than for FRF magnitude. For instance, although for simulation C350 FRF provides changes over 16%, V_d provides changes around 970%.

TABLE 1 Values of index ID_i at different levels of damage on the WPDs of the FD specimen

	Level of damage			
Damper	**d0**	**d1**	**d2**	**d3**
FD ground floor I1	0.00	0.17	0.45	0.77
FD ground floor I2	0.00	0.12	0.42	0.78
FD first floor I1	0.00	0.03	0.07	0.12
FD first floor I2	0.00	0.03	0.06	0.12

ID = index of damage; WPD = web plastifying damper.

TABLE 2 Values of index ID_i at different levels of damage on the WPDs of the SD specimen.

	Level of damage					
Damper	**d0**	**d1**	**d2**	**d3**	**d4**	**d5**
SD ground floor	0.00	0.01	0.06	0.31	0.76	1.15
SD first floor	0.00	0.02	0.05	0.15	0.27	0.40

WPD = web plastifying damper.

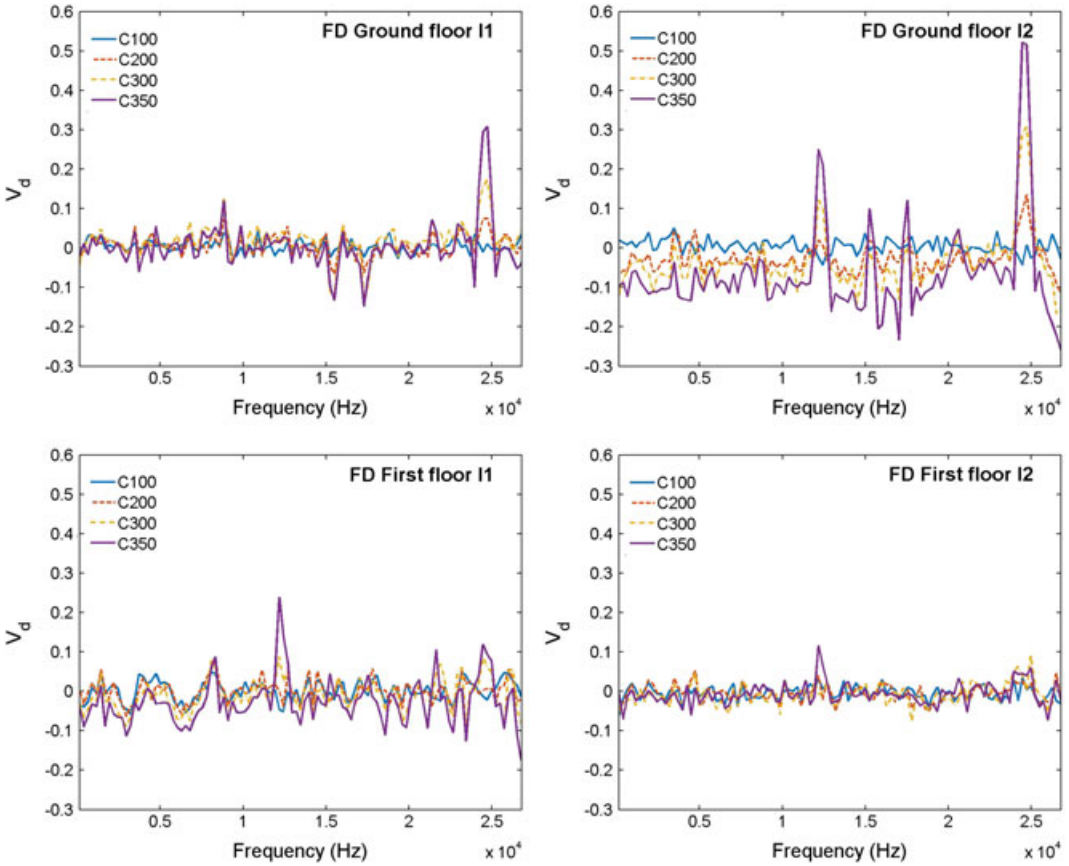

FIGURE 6 V_d versus frequency for I-sections of FD specimen

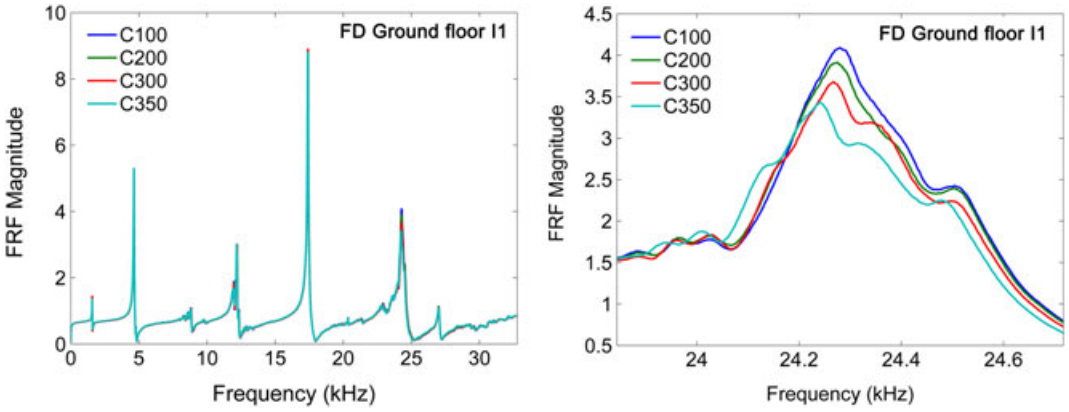

FIGURE 7 Frequency response function (FRF) versus frequency for I-section I1 located on the ground floor of the specimen FD, in the whole spectral range and zoomed to the fifth resonance

Figure 8 shows the results obtained for the four I-sections located on specimen SD. In both cases of study, the V_d and WER index were higher at the ground floor than at the first floor, indicating that the greatest damage was concentrated on the ground floor.

The WER index of the WPDs was calculated as explained above for the different levels of damage. The values of WER indexes obtained for each specimen at the end of each seismic simulation are given as subindices that indicate the name of the specimen (FD or SD) followed by the scaling factor of the acceleration applied to the shaking table (100%, 200%, 300%, and 400% for specimen FD, and 100%, 200%, 300%, 400%, 500%, and 600% for specimen SD). These values can be arranged in two vectors as follows:

$$WER_{FD} = [WER_{FD100}\ WER_{FD200}\ WER_{FD300}\ WER_{FD350}]$$
$$WER_{SD} = [WER_{SD100}\ WER_{SD200}\ WER_{SD300}\ WER_{SD400}\ WER_{SD500}\ WER_{SD600}].$$

In order to establish the reliability of the proposed index, a comparison with the mechanical damage index ID was carried out. First, the comparison was made for each repetition of the vibration test (T1, T2, T3, and T4) at each level of damage of the I-section steel segments of specimen FD, and for T1, T2, and T3 of the I-section steel segment of specimen SD. The results are shown in Figures 9 and 10, respectively. It can be observed that WER index follows well the behavior of the ID index as the level of damage increases, and that no important differences exist between the different repetitions of the vibration tests in each case.

Finally, Figure 11 presents the WER-ID plots grouping the four I-sections of each specimen. Each point of this plot is an average over the repetitions of the vibration test. The I-section segments used for the specimen FD and for the specimen SD were not cut from the same steel profile. As a result and due to the tolerances allowed in the production of

TABLE 3 FRF magnitude and V_d magnitude for I-section I1 located on the ground floor of the specimen FD, at different damage levels and its variation (%) respect to the seismic simulation C100.

		Variation respect to C100		Variation respect to C100
	FRF magnitude	ΔFRF magnitude (%)	V_d magnitude	ΔV_d magnitude (%)
C100	4.093	0.00	0.028	0
C200	3.914	−4.37	0.0762	172.14
C300	3.681	−10.07	0.1686	502.14
C350	3.435	−16.08	0.3008	974.29

FRF = frequency response function

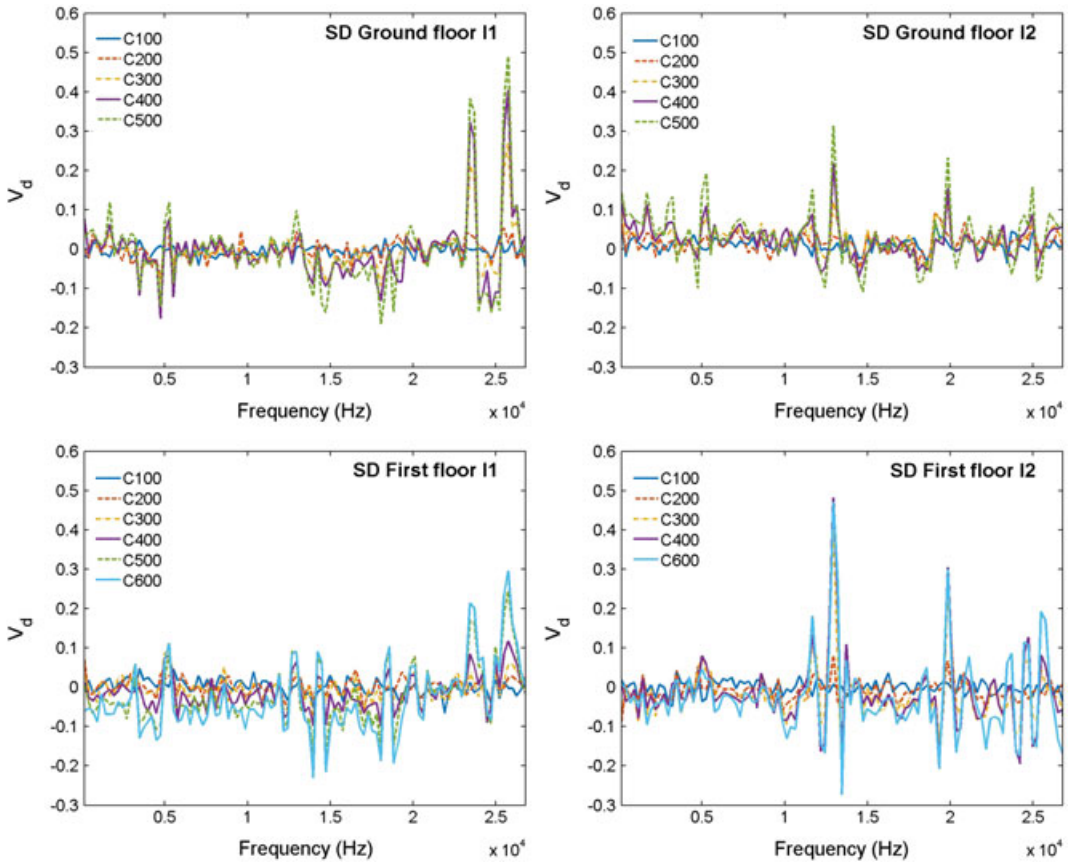

FIGURE 8 V_d versus frequency for I-sections of specimen SD

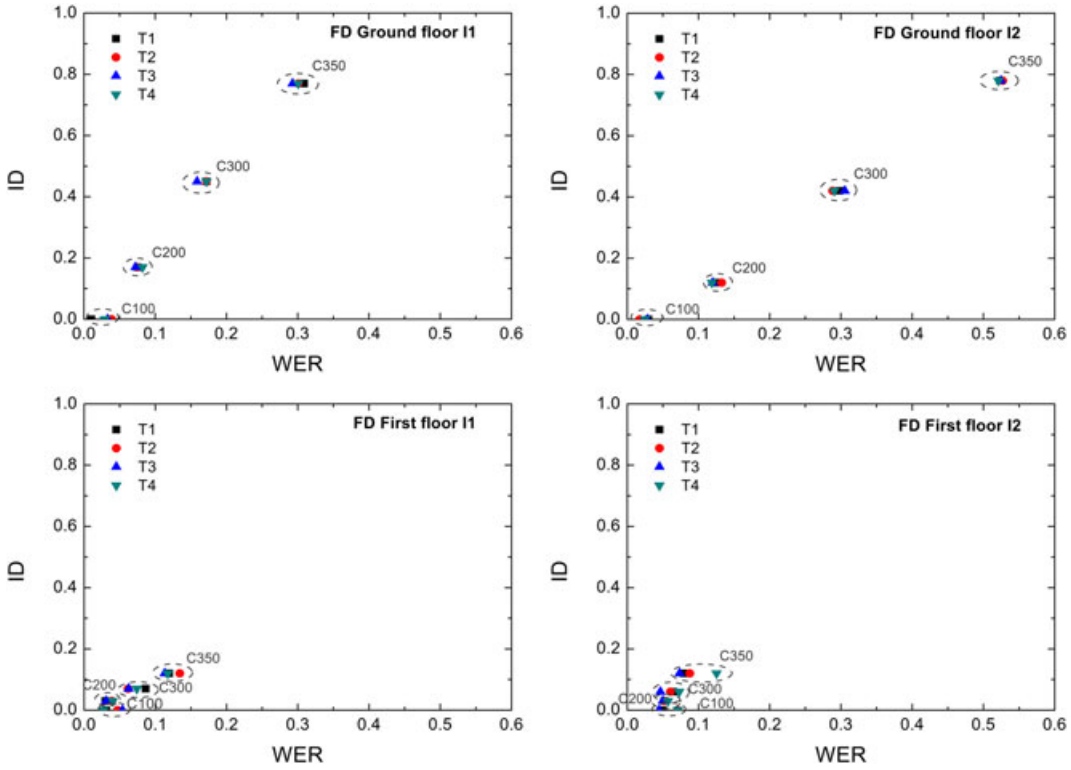

FIGURE 9 ID versus wavelet energy ratio (WER) for each I-section of the dampers of specimen FD

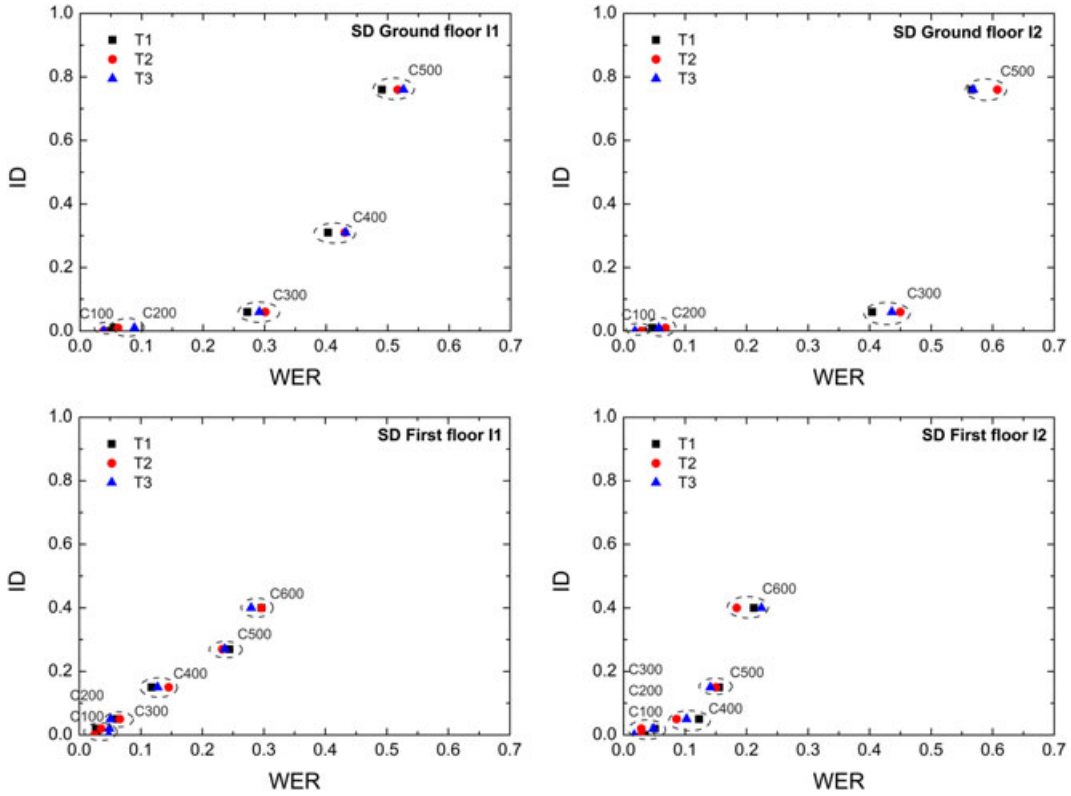

FIGURE 10 ID versus wavelet energy ratio (WER) for each I-section of the dampers of specimen SD

hot-rolled steel profiles, the dimensions of the I-segments used in both specimens were not exactly the same. This is the reason why the correlation between WER and ID indexes is different for specimen FD and for specimen SD and are shown in two different plots in Figure 11. Linear fitting and correlation coefficients are given in each case. Results are

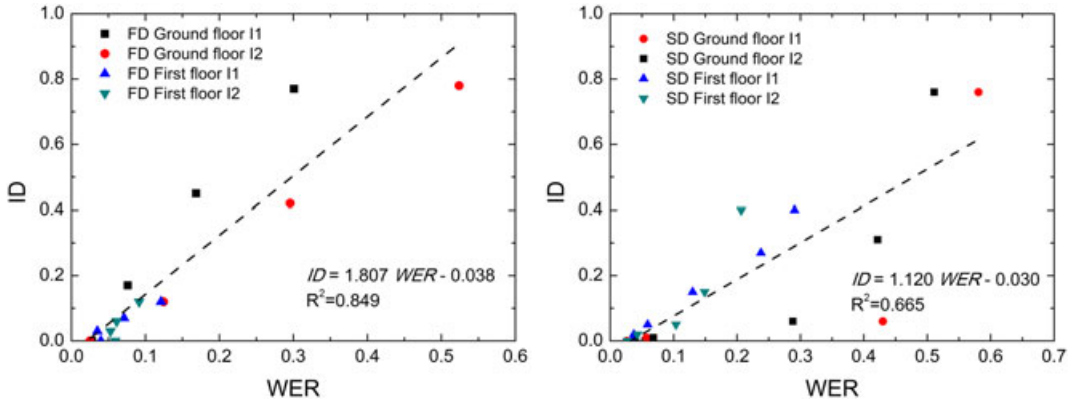

FIGURE 11 ID versus wavelet energy ratio (WER) for dampers of specimens FD (left) and SD (right)

in general very satisfactory, especially for specimen FD. From this correlation between the ID and WER indices, ID can be directly obtained from the WER index, and this presents two important advantages: (a) no real-time data recordings during the earthquake are needed and (b) the required instrumentation is simpler and cheaper.

6 | CONCLUSIONS

A new index called wavelet energy ratio (WER) has been proposed to quantify the damage on hysteretic dampers subjected to random seismic-type dynamic loadings. The WER index is based on wavelet package decomposition of the signals obtained from simple vibration tests. The validity of the WER index was assessed experimentally by testing a particular type of hysteretic damper called WPD on a shaking table. To this end, several WPDs were installed in two different reinforced concrete structures (a frame structure and a flat-plate structure) and the entire system was subjected to several seismic simulations of increasing magnitude. The damage accumulated in the WPDs at the end of each seismic simulation was quantified using two indices. One is the mechanical damage index ID proposed in past research, which has been extensively calibrated with the results of static and dynamic tests. The main drawback of the ID index is that its calculation calls for knowing the load–displacement curve endured by the hysteretic damper during the seismic event. The other is the WER index, proposed in this study, which relies on the output signals obtained from low-amplitude vibration tests conducted on the dampers after each seismic simulation. It was found that the proposed WER index correlates very well with the ID index. This enables one to assess the damage on hysteretic dampers without resorting to the cumbersome and expensive instrumentation required for in situ continuous monitoring of the dampers.

ACKNOWLEDGEMENTS

This research received the financial support of the local government of Spain, Consejería de Economía, Innovación y Ciencia, Projects P07-TP-02610 and P12-TEP-2429.

REFERENCES

[1] A. Benavent-Climent, *Earthq. Eng. Struct. Dyn.* **2007**, *36*(8), 1049, https://doi.org/10.1002/eqe.671.

[2] A. Gallego, A. Benavent-Climent, L. Romo-Melo, *Mech. Syst. Signal Process.* **2015**, *60-61*, 90, https://doi.org/10.1016/j.ymssp.2015.01.030.

[3] A. Benavent-Climent, A. Gallego, L. Romo-Melo, L. Morillas, *Struct. Health Monit.* **2014**, *13*(1), 33, https://doi.org/10.1177/1475921713499273.

[4] L. Romo, A. Benavent-Climent, L. Morillas, D. Escolano, A. Gallego, *Earthq. Struct.* **2015**, *8*(3), 485, https://doi.org/10.12989/eas.2015.8.3.485.

[5] L. Romo. Diagnóstico de daño en disipadores de energía histeréticos usados como sistema de control pasivo en estructuras sismorresistentes, mediante técnicas de procesamiento digital de señales de vibraciones. *PhD thesis*; University of Granada, Spain, **2012**.

[6] K. Worden, G. Manson, *J. Sound Vib.* **2003**, *259*(2), 323, https://doi.org/10.1006/jsvi.2002.5168.

[7] S. Fassois, J. Sakellariou, *The Royal Society-Philos. Trans. Math. Phys. Eng. Sci.* **2007**, *365*, 411, https://doi.org/10.1098/rsta.2006.1929.

[8] A. Benavent-Climent, L. Morillas, J. M. Vico, *Earthq. Eng. Struct. Dyn.* **2011**, *40*, 473.

[9] P. Chiariotti, M. Martarelli, G. M. Revel. Delamination detection by multi-level wavelet processing of continuous scanning laser Doppler vibrometry data optics and lasers in engineering **2017**; In Press (Available online).

[10] B. Asgarian, V. Aghaeidoost, H. R. Shokrgozar, *Mar. Struct.* **2016**, *45*, 1.

[11] L. Han, C. W. Li, S. L. Guo, X. W. Su, *Mech. Syst. Signal Process.* **2015**, *62-63*, 91.

[12] A. Y. Goharrizi, N. Sepehri, *Int. J. Fluid Power* **2014**, *14*(2), 39, https://doi.org/10.1080/14399776.2013.10781074.

[13] X.-L. Peng, H. Hao, Z.-X. Li, *Eng. Struct.* **2012**, *39*, 50.

[14] H. Y. Noh, K. K. Nair, D. G. Lignos, A. S. Kiremidjan, *Am. Soc. Civil Eng.* **2011**, *137*, 1215.

[15] Z. Guosheng, L. Jiang, Z. Kui, *Min. Sci. Technol. (China)* **2011**, *21*(1), 35.

[16] Y.-Y. Liu, J. Yong-Feng, C.-D. Duan, X.-F. Zhao, *Eng. Appl. Artif. Intell.* **2011**, *24*(1), 87.

[17] Y. Feng, F. S. Schlindwein, *Mech. Syst. Signal Process.* **2009**, *23*(3), 712.

[18] S. Ekici, S. Yildirim, M. Poyraz, *Expert Syst. Appl.* **2008**, *34*(4), 2937.

[19] C. Junsheng, Y. Dejie, Y. Yu, *NDT&E Int.* **2005**, *38*, 569.

[20] H. Jian-Gang, R. Wei-Xin, *Int. J. Solids Struct.* **2005**, *42*(26), 6610.

[21] S. S. Law, X. Y. Li, X. Q. Zhu, S. L. Chan, *Eng. Struct.* **2005**, *27*(9), 1339.

[22] Y. J. Yan, H. N. Hao, L. H. Yam, *Int. J. Solids Struct.* **2004**, *41*, 6661.

[23] Y. J. Yan, L. H. Yam, *Comput. Struct.* **2004**, *82*(4–5), 347.

[24] N. G. Nikolaou, I. A. Antoniadis, *NDT&E Int.* **2002**, *35*, 197.

[25] A. Benavent-Climent, L. Morillas, D. Escolano-Margarit, *Earthq. Eng. Struct. Dyn.* **2014**, *43*, 2399, https://doi.org/10.1002/eqe.2459.

[26] A. Benavent-Climent, J. Donaire-Avila, E. Oliver-Saiz, *Earthq. Eng. Struct. Dyn.* **2016**, *45*, 315.

[27] S. Mallat, *A wavelet tour of signal processing*, 2nd ed., Academic Press, London, UK **1999**.

[28] Z. Sun, C. C. Chang, *ASCE J. Struct. Eng.* **2002**, *128*(10), 1354, https://doi.org/10.1061/(ASCE)0733-9445(2002)128:10(1354).

[29] S. Mallat, *IEEE Trans. Pattern Anal. Mach. Intell.* **1989**, *11*, 674.

[30] I. Daubechies, *Ten lectures on wavelets*, Society for Industrial and Applied Mathematics, Philadelphia, PA **1992**.

[31] C. K. Chui, *Wavelets: A mathematical tool for signal processing*, SIAM monographs on mathematical modeling and computation, Philadelphia, PA **1997**.

[32] A. Primer, *Introduction to wavelets and wavelet transforms*, Prentice Hall, Upper Saddle River, NJ **1998**.

[33] A. Jensen, A. la Cour-Harbo, *Ripples in mathematics: The discrete wavelet transform*, Springer, Berlin **2001**.

How to cite this article: Suarez E, Benavent-Climent A, Molina-Conde R, Gallego A. Wavelet energy ratio index for health monitoring of hysteretic dampers. *Struct Control Health Monit*. 2017;e2071. https://doi.org/10.1002/stc.2071